A GENERIC ROBUST MODEL-BASED ESTIMATOR FOR ACTIVE DAMPING OF SINGLE-PHASE GRID-TIED INVERTERS

Arthur de Abreu Romão[1], Newton da Silva[2]
State University of Londrina (UEL), Londrina – Paraná, Brazil
e-mail: [1]arthur.romao@outlook.com, [2]newton.silva@uel.br

***Abstract* – This paper presents the design and analysis of a signal estimator with improved robustness applied in the active damping (AD) of a single-phase grid-tied inverter with LCL low-pass filter. The proposed estimator is based on the mathematical model of the LCL filter, with resistors in series with the converter-side inductor and capacitor for improving robustness. The implementation method is also capable of estimate multiple filter signals. The control strategy presented uses a virtual resistor based AD, that suppresses the resonance ensuring stability and robustness, helping comply with power quality standards, such as IEEE 1547 and IEC 61727. The signal necessary for achieving the AD is obtained through the estimator, dismissing the use of additional sensors. The current control structure uses grid-side current feedback with proportional-resonant controller and harmonic compensation. The system is designed by the root locus approach to achieve stability despite grid parameter variance. The estimator and overall system is analyzed through mathematical modeling, computational simulation and experimental setup. The results show that the estimator presented is capable of providing the necessary AD feedback signal, even with grid inductance variation.**

***Keywords* – Control, Current Estimator, Grid-Connected Inverters, Power Quality, Renewable Energy, Stability.**

I. INTRODUCTION

The grid-tied voltage-source inverters (VSI) are widely used with renewable energy sources and distributed generation (DG) systems, being typically connected with a low-pass filter to the main grid, in order to reduce the current harmonics caused by pulse width modulation (PWM), and therefore meeting the energy quality requirements [1].

The necessity for inverters with improved efficiency and reduced volume led to the use of higher order low-pass filters, such as the inductive-capacitive-inductive (LCL) [2], although it presents a resonance which should be suppressed in order to avoid energy quality degradation and ensure the system stability [2], [3].

To suppress the resonance in higher order filters, different damping techniques are presented in the literature, each with particular advantages and disadvantages. Some examples of resonance suppression strategies are: the passive damping (PD) [4], [5], which places passive elements within the filter, however, it reduces the system efficiency by providing damping through energy dissipation and can also prejudice the filter frequency response. The notch AD [6], which places a notch filter in the current control structure tuned to the resonant frequency value, although it improves efficiency the robustness is compromised, needing more complex adaptive notch filter schemes to ensure damping in connection to grids with large inductance variations [7]. The virtual resistor AD [8],[9] presents high efficiency and robustness, but it is usually necessary additional measurement for obtaining the damping signal feedback, commonly, the feedback signal used for AD is the LCL capacitor current or voltage, elevating the cost and hardware complexity due to additional sensors.

Different methods have been proposed in the literature aiming at eliminate the need of additional sensors for obtaining the virtual resistor AD. Some authors uses the same feedback signal for both control and AD [10], although, if using the grid-side current feedback, it is necessary the application of derivative filters, which can be difficult to implement due to the amplification of higher frequencies [9],[10]. Other works present the use of observers [11],[12], in this case the authors show that the observer reduces robustness to grid inductance variations [11]. The current estimation for AD using digital filters has also been suggested [13], showing improvements in robustness, however, it uses two second-order digital filters in order to estimate only one specific LCL filter variable, presenting limited application.

The AD method used is a virtual resistor in series with the converter-side inductor, due to its harmonic rejection capabilities, therefore, it needs the feedback of the converter-side current to perform the AD with a proportional gain [10].

In this context, the present paper aims to describe, analyze and design a novel generic estimator based on the model of a LCL filter with series damping resistors in both converter-side inductor and capacitor, improving robustness to grid inductance variation. The proposed estimator is then applied in the reconstruction of converter-side current for the AD of a grid-tied VSI with LCL filter. Furthermore, it will be presented in section V, that the the estimated current shows fewer high frequency components, resulting in a cleaner signal. Also, the generic estimator described is capable of reconstruct multiple variables of the LCL filter, therefore, it can be applied for different situations besides AD, such as using an estimated capacitor voltage for reducing current spikes in the moment of grid connection [14].

The estimator parameters, virtual resistor value and control gains are designed by a z-plane root locus plot aiming to obtain a good stability margin. The virtual resistor is placed in series with the converter-side inductor, providing assistance in the

Manuscript received 07/21/2021; first revision 11/12/2021; accepted for publication 02/02/2022, by recommendation of Editor Marcelo Lobo Heldwein. http://dx.doi.org/10.18618/REP.2022.1.0038.

attenuation of undesirable harmonics, where this configuration can be achieved through feedback of the converter-side current with a proportional gain [10].

The current control is performed by a proportional-resonant (PR) controller with harmonic compensation (HC) with an alternative topology [15], using the grid-side current for feedback, resulting in low steady-state error [16].

This paper is structured in seven sections. Section II presents the overall system and control structure used for the estimator and AD analysis. Section III describes the LCL filter and estimator structure. Section IV shows the design procedure for the controller and estimator parameters. Section V brings the simulation and experimental results, and, finally, Section VI presents the final remarks.

II. SYSTEM DESCRIPTION

The control structure and overall system is presented in Figure 1. It contains a DC powered single-phase VSI connected to the main grid by an LCL filter.

The current reference structure, presented in Figure 1, contains a phase-locked-loop (PLL) for grid synchronization, producing a sinusoidal signal synchronized with the grid voltage signal (V_g). This resulting sinusoidal signal is then combined with the current amplitude value, provided by a power control, based on DC-link voltage, thus producing the reference current signal (i_{ref}).

The current control structure depicted in Figure 1 is based on proportional-resonant (PR) controller with harmonic compensation (HC), with an alternative topology that improves harmonic rejection, if compared to the standard PR with HC scheme [15]. The resonant controller ($R(s)$) and HC with proportional gain ($PR_h(s)$) transfer functions are presented in equations (1) and (2), respectively.

$$R(s) = K_r \frac{s}{s^2 + \omega_g^2} \tag{1}$$

$$PR_h(s) = K_p + \sum_{h=3,5,7...} \frac{K_{rh} s}{s^2 + (h\omega_g)^2}. \tag{2}$$

Where ω_g is the main grid frequency in rad/s, h the order of harmonic component and K_p, K_r and K_{rh} the control gains.

The resonant controller applied in the current control is widely used in grid tied systems due to the ability to eliminate the steady-state error between the controlled signal and its sinusoidal reference [16]. Although, unlike conventional PR controllers, this structure uses the grid-current (i_o) feedback in the comparison with current reference signal, for generating the error signal for compensation, and also directly in the HC control [15]. The compensated error signal, which is the current control structure output, is subtracted by the AD signal, which results in the duty-cycle signal (d) after the PWM block.

The discretization for implementation in a digital signal controller (DSC) is done using impulse invariant method, in order to better preserve the resonant filter characteristics [17]. The controller gains for obtaining a stable response is defined in Section IV through the root locus approach.

The AD signal is generated by processing a feedback variable, obtained from the LCL filter. The type of signal processing applied to a specific feedback variable defines the kind of PD scheme that the virtual resistor AD will emulate [10].

In order to obtain the feedback signal for performing the AD, a generic damped model-based estimator is employed. The estimator uses grid-current (i_o), DC-link voltage (v_{dc}) and reference voltage (v_{ref}) as the input signals for reconstructing the remaining LCL filter variables, such as the converter-side current necessary for the desired virtual resistor AD. The estimator is detailed in the following sections.

The LCL filter design [18], considers the ratio between switching and resonance frequency values, for this system the switching frequency is set to, approximately, 4.5 times the resonance frequency at strong grid condition, in order to improve the virtual resistor AD performance and the high frequencies attenuation [19]. Also, both inductors are set to the same value, as to attain robustness to grid inductance variation with small voltage drop in the grid-side inductor [18].

The inverter is rated for an apparent power of 400 VA, with an effective grid voltage of 115 V, therefore, the DC-link voltage value must consider realistic losses, such as switches and passive elements. For this reason, its value is set to 10 % above the peak grid voltage, to 180 V. The weak grid equivalent inductance considers a value of 1 mH, and for the strong grid case the equivalent inductance is considered as ideal, thus, 0 mH.

With those considerations taken, the overall system parameters are shown in Table I.

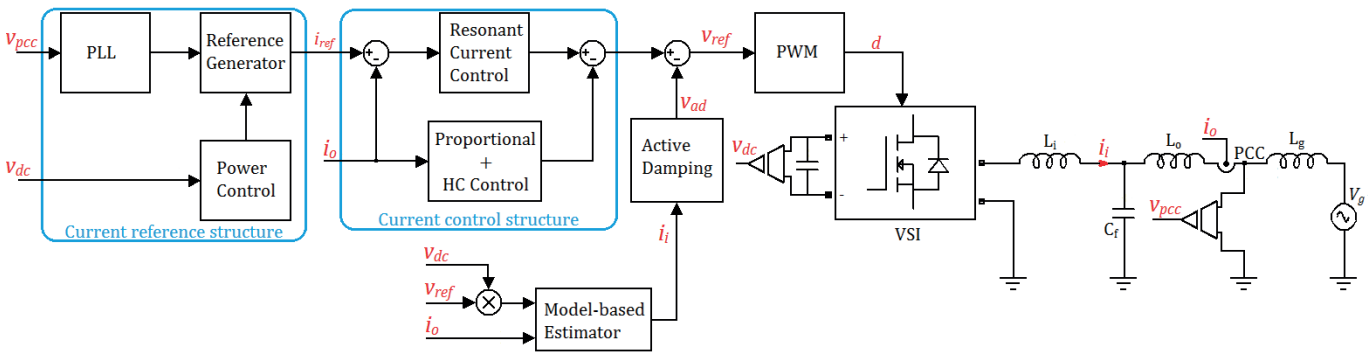

Fig. 1. System with signal estimator structure for AD in single-phase grid connected inverter.

TABLE I
System Parameters

Parameter	Symbol	Value
Inverter side LCL filter inductance	L_i	1.4 mH
Grid side LCL filter inductance	L_o	1.4 mH
LCL filter capacitance	C_f	4 μF
Weak grid equivalent inductance	L_g	1 mH
Strong grid equivalent inductance	L_g	0 mH
Effective grid voltage	V_g	115 V
DC bus voltage	v_{dc}	180 V
Rated inverter apparent power	S_n	400 VA
Grid frequency	f_g	60 Hz
Switching frequency	f_s	14400 Hz
Resonance frequency (strong grid)	f_r	$\approx$ 3100 Hz
Resonance frequency (weak grid)	f_r	$\approx$ 2600 Hz

III. LCL FILTER MODELING AND ESTIMATOR STRUCTURE

The LCL filter model is derived from the presented circuit diagram in Figure 2, considering the VSI and grid connection.

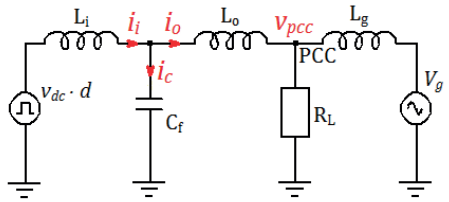

Fig. 2. Equivalent circuit of the grid-tied VSI with LCL filter.

For the analysis of the circuit in Figure 2, the local load (R_L) is seen as an infinite resistance and only the VSI input voltage is regarded, consequently, $V_g = 0$, with the DC-link voltage (v_{dc}) as a constant value. Therefore, by solving the circuit in frequency domain, taking the duty-cycle (d) as the input signal, and grid-side current (i_o) as the output variable, the transfer function in equation (3).

$$G_p(s) = \frac{i_o(s)}{d(s)} = \frac{\frac{v_{dc}}{L_i C_f (L_o + L_g)}}{s^3 + \frac{L_i + L_o + L_g}{L_i C_f (L_o + L_g)} s}. \quad (3)$$

The resonance frequency (ω_r) is characterized by the poles in (3), and it is defined in equation (4).

$$\omega_r = \sqrt{\frac{L_i + L_o + L_g}{L_i C_f (L_o + L_g)}}. \quad (4)$$

Equation (4) presents the frequency where transfer function (3) shows infinite gain, which can lead to an increase in the total harmonic distortion (THD) and, in extreme cases, instability [19]. Therefore, a damping factor introduced in the denominator of (3) can ensure a proper system operation, improving energy quality and ensuring stability.

The LCL filter circuit presented in Figure 2 can also be understood in terms of block diagram, as shown in Figure 3, without the connection of a local load in the PCC. This representation is useful for modeling PD and AD methods [10], as the passive impedances are represented individually, which can then be associated with damping resistors, and all the filter current and voltage variables are accessible for virtual resistor techniques.

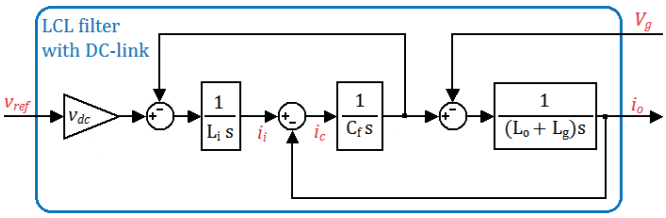

Fig. 3. VSI and LCL filter represented in the form of block diagram.

A. Damped Model-based Estimator Structure

The structure presented in Figure 3 is used in the implementation of a generic signals estimator for the LCL filter.

The elements that represent the passive components must be discretized for application in a DSC and an unit delay has to be inserted in the feedback loop, as shown in Figure 4, in order to compensate the first sample absence and be practical in digital control systems. The unit delay is approximated in s-domain by the Padé approximation [20], shown in equation (5).

$$e^{-\frac{s}{f_s}} \approx \frac{f_s - 0.5s}{f_s + 0.5s}. \quad (5)$$

Also, for the estimator to provide the signals correctly it have to be stable and, moreover, it should be able to deal with equivalent grid inductance variation, in order to maintain the correct estimation of filter variables [13]. As for the actual LCL filter, the insertion of a damping factor ensures stability and improves THD [10].

The estimator depicted in Figure 4 presents the passive elements models with the addition of a series damping resistor, in the s-domain. To implement on DSC the estimator is discretized by Tustin method, preserving its frequency response characteristics. The input signals considered for the reconstruction of other variables are the grid-side current, which is also used in the current control structure, and the reference voltage (v_{ref}), which is an internal variable provided as the result of control and AD, combined with the DC bus voltage (v_{dc}).

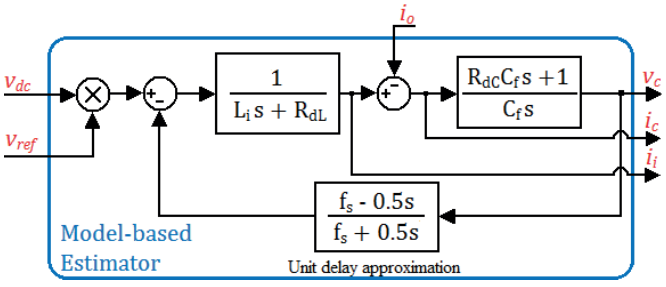

Fig. 4. Generic damped model-based estimator for LCL filter with grid-side current, voltage reference and DC bus voltage as inputs.

The equivalent circuit of the estimator shown in Figure 4 is presented in Figure 5, having a resistor in series with the converter-side inductor and also with the capacitor. This configuration shows better robustness and stability, as presented in details in Section IV.

Therefore, the estimator presented reconstructs the LCL filter variables by the implementation of the mathematical model structure of the filter, presented in Figure 4, in the DSC,

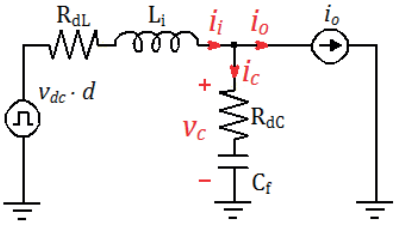

Fig. 5. Equivalent circuit of the generic damped estimator for LCL filter.

and by feeding the estimator with the DC-link voltage (v_{dc}), reference voltage (v_{ref}) and grid-side current (i_o) it is possible to obtain the remaining variables present in the LCL filter that were not directly measured.

The converter-side current (i_i) signal, that is accessed in the estimator as depicted in Figure 4, is used in this work to attain the virtual resistor AD [10], and the capacitor voltage signal, that is also a result from the estimators processing, can be applied to obtain softer grid connection [14].

B. Series Virtual Resistor AD LCL Filter

The damping of the actual LCL filter is done by placing a virtual series resistor with the converter-side inductor. This AD method is achieved through the feedback of the converter-side current [10], as shown in Figure 6, however, for this study, the needed current to perform the AD is obtained indirectly, through estimation, as presented in Figure 1.

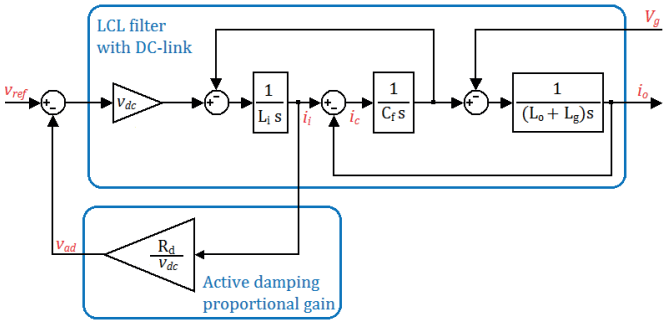

Fig. 6. Block diagram of series virtual resistor active damping.

The structure presented in Figure 6 is equivalent to the circuit shown in Figure 7.

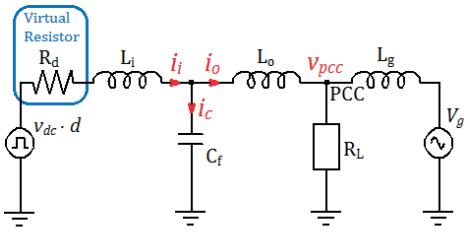

Fig. 7. Equivalent circuit of the grid-tied VSI with virtual resistor series AD in LCL filter converter-side inductor.

The configuration in Figure 7 acts not only suppressing the resonance, by adding a damping coefficient to the filter transfer function, but also introduces an attenuation proportional to the damping virtual resistor value (R_d) in the lower frequencies, as shown by equation (6), hence, helping in the rejection of lower harmonic components that are not tuned in the HC filters.

$$G_{p\_sd}(s) = \frac{i_o(s)}{d(s)} = \frac{\frac{v_{dc}}{L_i C_f (L_o + L_g)}}{s^3 + \frac{R_d}{L_i} s^2 + \omega_r^2 s + \frac{Rd}{L_i C_f (L_o + L_g)}}. \quad (6)$$

In order to obtain the damping factor value for the transfer function in equation (6), as a mean to design the damping resistor value, it is approximated that the AD does not affect the resonance frequency value (ω_r). Thus, by decomposing equation (6) and comparing it with a general second-order system, presented in equation (7) [21], results in the approximated damping factor shown in equation (8), for strong grid condition.

$$H(s) = \frac{K\omega_r^2}{s^2 + 2\zeta\omega_r s + \omega_r^2} \quad (7)$$

$$\zeta_s \approx \frac{R_d}{4\omega_r L_i}. \quad (8)$$

IV. CONTROL PARAMETERS DESIGN

A. Generic Model-based Estimator

The design of damping parameters for the estimator is done through root locus plot in z-domain, by the discretization with Tustin method of the structure presented in Figure 4, considering strong grid condition as standard.

This design is done in two steps: the first root locus considers the resistor R_{dC} as zero, and the value of R_{dL} is chosen as to ensure the estimator stability; the second step uses root locus to design R_{dC}, with the value of R_{dL} obtained previously, choosing the poles in order to further increase robustness. The estimator considers both series resistors as means to improve robustness to parameter variation.

The root locus for designing R_{dL} is presented in Figure 8.

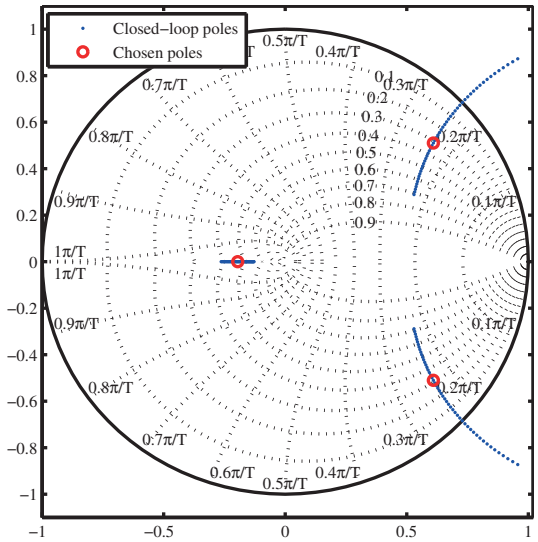

Fig. 8. Root locus for estimators R_{dL} design.

The value of R_{dL} that results in the poles chosen in Figure 8 is $R_{dL} = 30\ \Omega$. This value was chosen aiming to provide the most stable closed-loop poles, being closest to the center of z-plane unitary circle, and so attaining better stability margin.

With R_{dL} defined, the root locus for designing R_{dC} is shown in Figure 9.

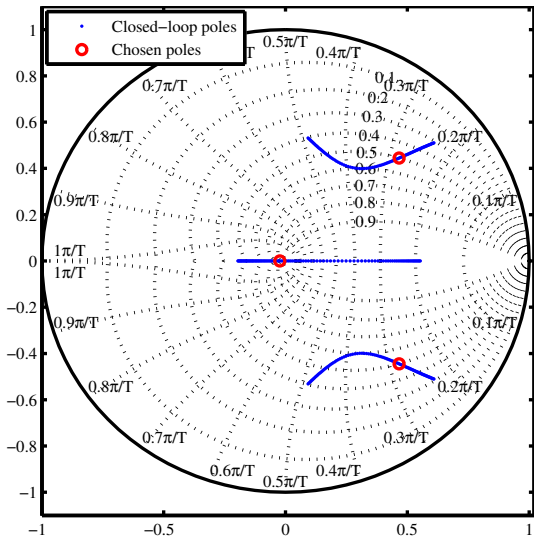

Fig. 9. Root locus for estimators R_{dC} design.

Therefore, the value of R_{dC} that results in the poles chosen in Figure 9 is $R_{dC} = 8\ \Omega$. The value of R_{dC} was chosen as to further improve stability margin, pushing the poles to the center of the z-plane unitary circle.

B. Virtual Resistor AD and Current Control

The virtual resistor design for obtaining the AD is done by defining a damping factor and applying it to the equation (8).

The suggested damping factor for PD techniques range between $0.1 \leqslant \zeta_s \leqslant 0.3$ [5], as this range provides sufficient damping with fewer losses. Although this paper proposes an AD, the mentioned damping factor range is used as a guideline, thus the value $\zeta_s = 0.25$ is chosen, and, from equation (8), it results in a virtual resistor of, approximately, $R_d = 26\ \Omega$.

With the virtual resistor R_d defined, the design of proportional control gain is done through the root locus presented in Figure 10. The value of $K_p = 0.04$ is chosen, resulting in the poles indicated in Figure 10, providing stability.

The resonant gain K_r can be chosen from a large range, since its value has little influence in stability [10], however, its value must be enough to provide minimum steady state error, therefore $K_r = 40$ meet this requirement. A smaller gain is viable to be set for K_{rh}, since the amplitude of harmonic components is smaller than the fundamental, consequently $K_{rh} = 10$ [13].

V. SIMULATION AND EXPERIMENTAL RESULTS

A. Estimator Analysis

In order to observe the estimator performance, a computational simulation is conducted in MATLAB®, based on the system described in Section II. The signals provided by the estimator is compared with the original signals, both in strong and weak grid condition, for robustness assessment.

The Figure 11 brings a comparison between the original capacitor voltage signal and converter-side current signal

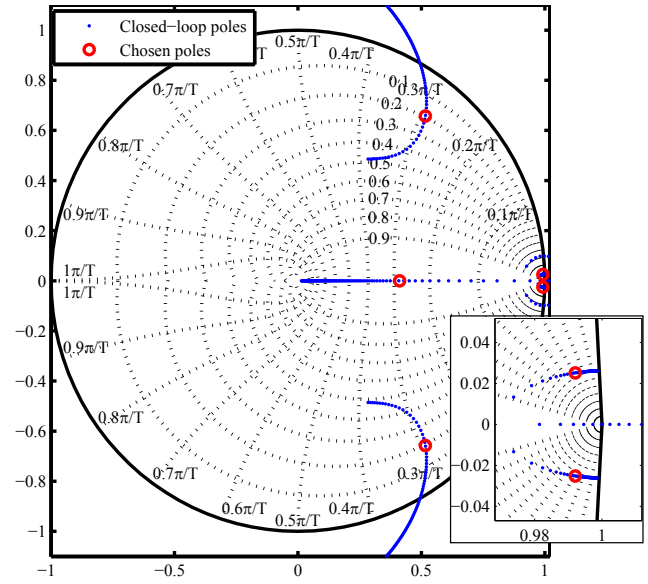

Fig. 10. Root locus for virtual resistor AD R_d design.

against its estimated counterparts, at strong grid condition. The grid-side current reference is set to 0.5 A peak.

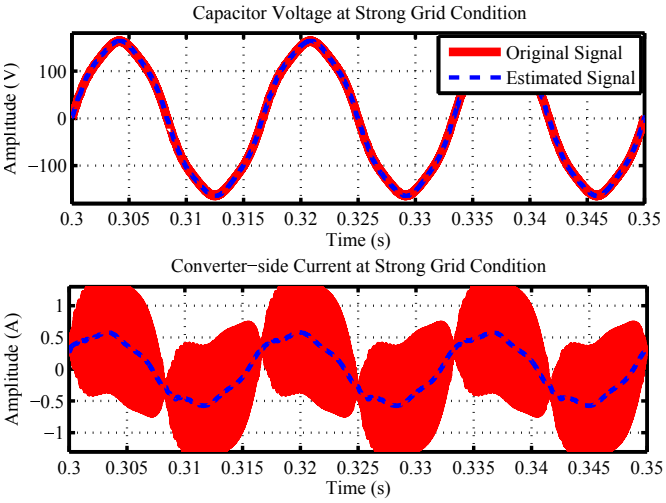

Fig. 11. Comparison between original and estimated signals at strong grid condition in simulation, for capacitor voltage and converter-side current, as noted.

From Figure 11 it is noticeable that the estimated capacitor voltage signal is almost identical to the original signal, with a slight delay. The converter-side original current presents the switching frequencies, as expected, the estimated signal shows only the lower frequencies components. This result shows that, in a simulated environment, the proposed estimator structure is capable of providing reconstructed signals coherent with the real ones.

The same experiment is conducted for the weak grid condition, presented in Figure 12.

The waveforms for the weak grid condition presented in Figure 12 are very similar to the result in Figure 11, showing that the estimator is able to deal with the grid equivalent inductance variation.

The comparison between estimated and original signals is also done in an experimental setup, that uses the DSC

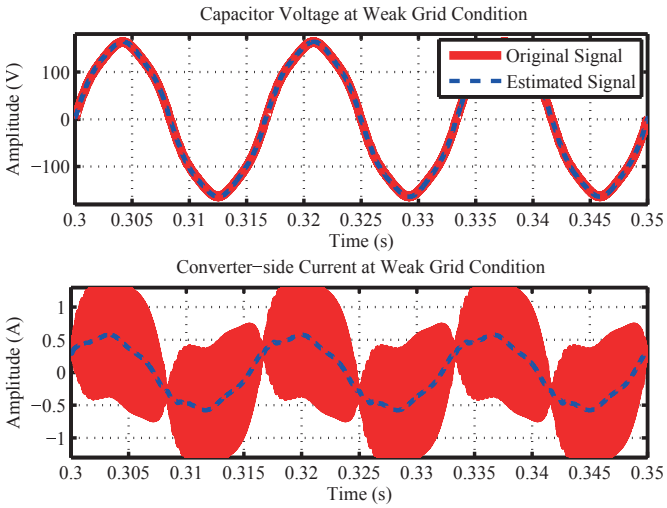

Fig. 12. Comparison between original and estimated signals at weak grid condition is simulation, for capacitor voltage and converter-side current, as noted.

TMS320F28335 for the control structure implementation, while the inverter uses IRF840 MOSFET switches triggered by TLP250 optocouplers. In Figure 13 it is presented the capacitor voltage, where the oscilloscopes channel 1 contains the original voltage signal and channel 2 the estimated voltage signal, in this experiment it is considered a weak grid condition.

Figure 14 shows the experimental converter-side current, in detail, with no load at the PCC. The channel 1 presents the original current signal and channel 2 the estimated current signal.

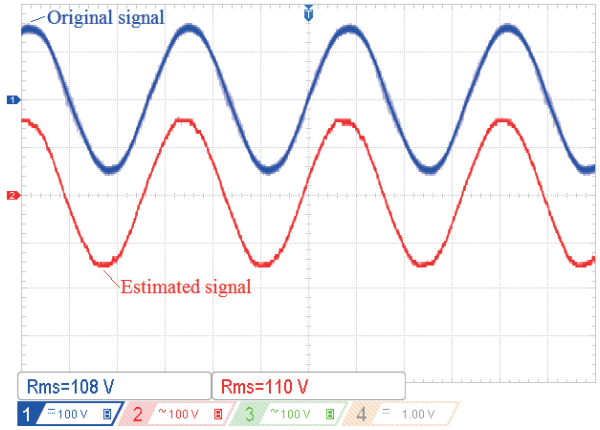

Fig. 13. Comparison between original and estimated capacitor voltage signal, in experimental prototype.

The experimental results shown in Figure 13 and 14 further confirms the ability of the proposed estimator to correctly reconstruct non-measured signals, as both show a similar behavior as observed in simulation: the estimated capacitor voltage signal being almost identical to the original one, despite a slight delay, and the estimated converter-side current containing the lower frequency components, whereas the original current also presents the switching frequency components. The ripple observed in the estimated converter-side current, in Figure 14, is a result of noise and frequency components present in the measured grid-side current, which

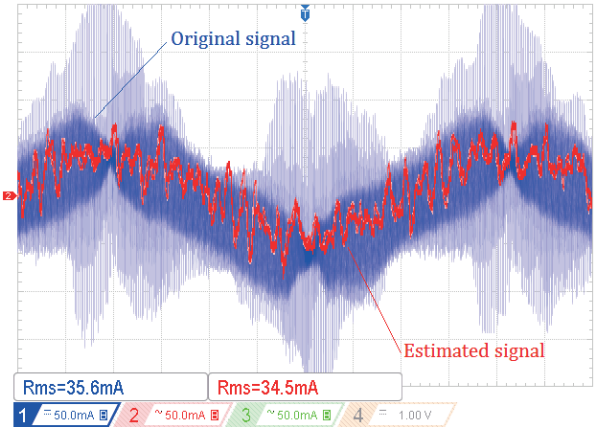

Fig. 14. Comparison between original and estimated converter-side current signal, in experimental prototype.

is carried through the estimator producing a ripple specially visible at low values of reference current.

B. System Output Analysis

The system grid-side current (i_o), presented in Figure 1, is analyzed through simulation at strong and weak grid conditions. The virtual resistor AD is achieved by the feedback of converter-side current reconstructed by the estimator presented in Figure 4. The active damped LCL filter is compared with the system without damping. The reference current is set to 0.5 A peak. The grid voltage contains the third and fifth harmonics, which is also the harmonic components the HC control is tuned to.

Figure 15 presents the grid-side current waveform at strong and weak grid conditions, from 0 to 0.35 seconds the AD is operative, from 0.35 to 0.4 seconds the AD is disabled.

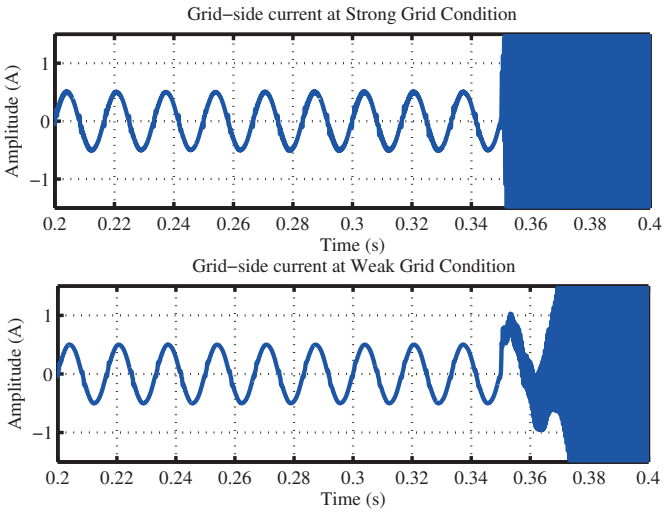

Fig. 15. Simulated grid-side current at strong and weak grid conditions.

Figure 15 shows that, for the simulated system, the absence of damping leads to instability, in both strong and weak grids. It is important to observe that with the AD enabled, the system remains stable for both grid cases, meaning that the AD with estimator is operating correctly despite the grid equivalent inductance variation.

The harmonic content for the signals presented in Figure 15

is shown in Figure 16.

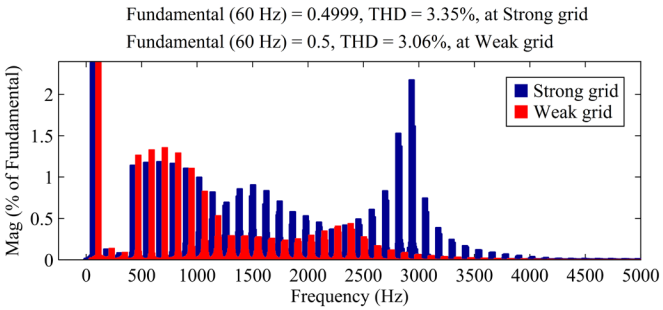

Fig. 16. Harmonic content of simulated grid-side current at strong and weak grid conditions.

For both strong and weak grid cases the THD is kept around 3%, although the strong grid scenario presents greater distortion, both results meet the power quality standard IEEE 1547 [22] limits, which is below 5%.

The experimental grid-side current result is presented in Figure 17, and its harmonic content in Figure 18, for strong grid, the reference current is set to 0.1 A initially and at approximately 0.05 seconds a step is applied in the reference, going from 0.1 to 0.2 A peak, the low value of reference is to better observe the harmonic distortion caused by the grid voltage. From 0.3 seconds the AD is disabled. As in the simulated environment, the experimental setup also has the HC tuned to the third and fifth harmonics.

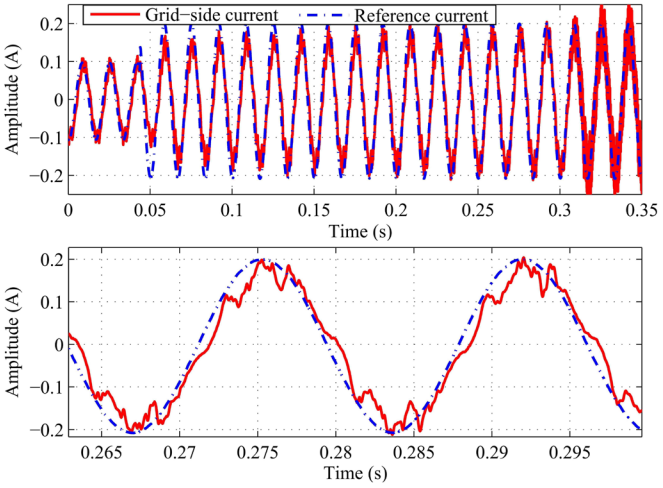

Fig. 17. Grid-side current in experimental setup.

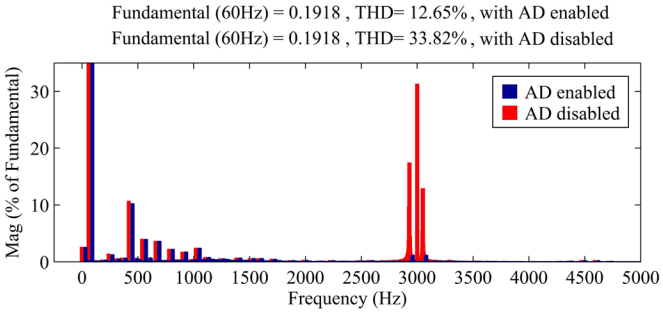

Fig. 18. Harmonic content comparison of grid-side current in experimental setup, with AD enabled and disabled.

The result presented in Figures 17 and 18 is coherent with the simulation presented in Figure 15, confirming that the virtual resistor AD using the proposed estimator is viable. The system presented a stable response to the reference current step, and the comparison between the AD, enabled and disabled, shows the effectiveness of the AD, with the harmonic components reaching 30% of the amplitude of fundamental without AD, significantly higher than the case with AD enabled.

Although it is noticeable a distortion caused by the seventh harmonic, the HC correctly compensates the third and fifth harmonics. The intrinsic resistances of the experimental prototype keeps the system stable without AD, and the grid voltage with components above the fifth harmonic elevates the THD of grid-side current,with AD, to 12.65%, and additionally, the lower current reference value chosen in the experimental setup also contributes to the higher THD than the observed in simulation.

VI. CONCLUSIONS

The presented generic damped model-based estimator proved to be capable of reconstructing close enough signals, compared to the original ones, as to obtain a virtual resistor AD without the need for additional measures, helping to make the inverters hardware simpler.

The design procedure for obtaining the estimators damping resistors showed good stability margin and robustness to grid inductance variation, being able to maintain the signals estimation and AD in both grid case scenarios studied.

Also, the implementation is of low complexity, needing two second order filters, that emulate both the LCL filter converter-side inductor and capacitor with a series resistor, in a feedback loop. With this configuration it is possible to obtain different filters variables, depending on the point of the estimator that signal in being read.

The experimental results confirm the effectiveness of the proposed signal estimation structure in reconstructing the variables, as the comparison between the estimated and original signals shows good correlation, and also in the obtainment of virtual resistor AD, as the experimental grid-side current shows stability and lower THD if compared with the case without AD, even in very low values of load.

ACKNOWLEDGEMENTS

The authors thank CAPES for the financial support.

REFERENCES

[1] A. Reznik, M. G. Simões, A. Al-Durra, S. M. Muyeen, "*LCL* Filter Design and Performance Analysis for Grid-Interconnected Systems", *IEEE Transactions on Industry Applications*, vol. 50, no. 2, pp. 1225–1232, March-April 2014, doi:10.1109/TIA.2013.2274612.

[2] P. S. N. Filho, T. A. S. Barros, M. G. Villalva, E. R. Filho, "Accurate Modeling for Analysis and Control Design of the DC-Side of the Grid-Tie VSC with LCL Filter", *Revista Eletrônica de Potência*, vol. 22, no. 1, pp. 7–18, March 2017, doi: 10.18618/REP.2017.1.2639.

[3] S. G. Parker, B. P. McGrath, D. G. Holmes, "Regions of Active Damping Control for LCL Filters", *IEEE Transactions on Industry Applications*, vol. 50, no. 1, pp. 424–432, January-February 2014, doi: 10.1109/TIA.2013.2266892.

[4] P. Channegowda, V. John, "Filter Optimization for Grid Interactive Voltage Source Inverters", *IEEE Transactions on Industrial Electronics*, vol. 57, no. 12, pp. 4106–4114, December 2010, doi: 10.1109/TIE.2010.2042421.

[5] R. Peña-Alzola, M. Liserre, F. Blaabjerg, R. Sebastián, J. Dannehl, F. W. Fuchs, "Analysis of the Passive Damping Losses in LCL-Filter-Based Grid Converters", *IEEE Transactions on Power Electronics*, vol. 28, no. 6, pp. 2642–2646, June 2013, doi: 10.1109/TPEL.2012.2222931.

[6] J. Dannehl, M. Liserre, F. Fuchs, "Filter-Based Active Damping of Voltage Source Converters With LCL Filter", *IEEE Transactions on Industrial Electronics*, vol. 58, no. 8, pp. 3623–3633, August 2011, doi: 10.1109/TIE.2010.2081952.

[7] M. Ciobotaru, A. Rossé, L. Bede, B. Karanayil, V. G. Agelidis, "Adaptive Notch filter based active damping for power converters using LCL filters", *in IEEE 7th International Symposium on Power Electronics for Distributed Generation Systems (PEDG)*, pp. 1–7, June 2016, doi:10.1109/PEDG.2016.7527081.

[8] D. Pan, X. Ruan, C. Bao, W. Li, X. Wang, "Capacitor-Current-Feedback Active Damping With Reduced Computation Delay for Improving Robustness of LCL-Type Grid-Connected Inverter", *IEEE Transactions on Power Electronics*, vol. 29, no. 7, pp. 3414–3427, July 2014, doi:10.1109/TPEL.2013.2279206.

[9] Z. Xin, P. C. Loh, X. Wang, F. Blaabjerg, Y. Tang, "Highly Accurate Derivatives for LCL-Filtered Grid Converter With Capacitor Voltage Active Damping", *IEEE Transactions on Power Electronics*, vol. 31, no. 5, pp. 3612–3625, May 2016, doi: 10.1109/TPEL.2015.2467313.

[10] T. Liu, J. Liu, Z. Liu, Z. Liu, "A Study of Virtual Resistor-Based Active Damping Alternatives for LCL Resonance in Grid-Connected Voltage Source Inverters", *IEEE Transactions on Power Electronics*, vol. 35, no. 1, pp. 247–262, January 2020, doi: 10.1109/TPEL.2019.2911163.

[11] M. A. Gaafar, G. M. Dousoky, M. Shoyama, "Robustness analysis for observer based active damping of LCL filter at different resonant frequencies", *in IEEE International Telecommunications Energy Conference (INTELEC)*, pp. 1–6, October 2015, doi: 10.1109/INTLEC.2015.7572390.

[12] M. Su, B. Cheng, Y. Sun, Z. Tang, B. Guo, Y. Yang, F. Blaabjerg, H. Wang, "Single-Sensor Control of LCL-Filtered Grid-Connected Inverters", *IEEE Access*, vol. 7, pp. 38481–38494, March 2019, doi:10.1109/ACCESS.2019.2906239.

[13] R. A. Liston, E. G. Carati, R. Cardoso, J. P. da Costa, C. M. O. Stein, "A Robust Design of Active Damping With a Current Estimator for Single-Phase Grid-Tied Inverters", *IEEE Transactions on Industry Applications*, vol. 54, no. 5, pp. 4672–4681, September-October 2018, doi:10.1109/TIA.2018.2838074.

[14] S. M. Machado, L. B. G. Campanhol, N. da Silva, I. A. I. Millán, "Grid-Connection strategy with reduced current spikes for grid-tie module-integrated converter", *in IEEE PES Innovative Smart Grid Technologies Conference - Latin America (ISGT Latin America)*, pp. 1–6, September 2017, doi: 10.1109/ISGT-LA.2017.8126688.

[15] S. J. M. Machado, R. A. F. Pereira, C. H. L. Oliveira, N. da Silva, "Enhancing harmonic rejection capability of grid-connected module-integrated converters", *in Brazilian Power Electronics Conference (COBEP)*, pp. 1–6, November 2017, doi:10.1109/COBEP.2017.8257371.

[16] R. A. S. Kraemer, E. G. Carati, J. P. da Costa, R. Cardoso, C. M. O. Stein, "Robust Design of Control Structure for Three-Phase Grid-Tied Inverters", *in 13th IEEE International Conference on Industry Applications (INDUSCON)*, pp. 636–643, November 2018, doi:10.1109/INDUSCON.2018.8627068.

[17] A. G. Yepes, F. D. Freijedo, J. Doval-Gandoy, O. López, J. Malvar, P. Fernandez-Comesaña, "Effects of Discretization Methods on the Performance of Resonant Controllers", *IEEE Transactions on Power Electronics*, vol. 25, no. 7, pp. 1692–1712, July 2010, doi:10.1109/TPEL.2010.2041256.

[18] R. Peña-Alzola, M. Liserre, F. Blaabjerg, M. Ordonez, Y. Yang, "LCL-Filter Design for Robust Active Damping in Grid-Connected Converters", *IEEE Transactions on Industrial Informatics*, vol. 10, no. 4, pp. 2192–2203, November 2014, doi: 10.1109/TII.2014.2361604.

[19] S. G. Parker, B. P. McGrath, D. G. Holmes, "Regions of Active Damping Control for LCL Filters", *IEEE Transactions on Industry Applications*, vol. 50, no. 1, pp. 424–432, January-February 2014, doi: 10.1109/TIA.2013.2266892.

[20] S. Buso, P. Mattavelli, *Digital Control in Power Electronics*, 2006, doi: 10.2200/S00047ED1V01Y200609PEL002.

[21] C. P. Basso, *Linear Circuit Transfer Functions: An Introduction to Fast Analytical Techniques*, pp. 41–115, May 2016, doi:10.1002/9781119236344.ch02.

[22] "IEEE Standard for Interconnection and Interoperability of Distributed Energy Resources with Associated Electric Power Systems Interfaces", *IEEE Std 1547-2018 (Revision of IEEE Std 1547-2003)*, pp. 1–138, April 2018, doi: 10.1109/IEEESTD.2018.8332112.

BIOGRAPHIES

Arthur de Abreu Romão, received BSc. in Electrical Engineer (2018) by State University of Londrina (UEL) and is currently a masters degree student in the State University of Londrina. His areas of interest are power electronics, grid-tied

inverters, digital control and energy quality.

Newton da Silva, received BSc. in Electrical Engineering (1991) from Federal University of Santa Maria, MSc. in Electrical Engineering (1994) from the Federal University of Santa Cataria (UFSC) and PhD. in Electrical Engineering (2012) from Unicamp. He has been a professor at the State University of Londrina (UEL), since 2003. His areas of interest are power electronics, power quality, grid-connected energy systems and digital control of converters.